NASA DEVELOP National Program
Massachusetts – Boston
Summer 2022

Great Slave Lake Water Resources

Mapping Long-Term Changes in the Hydroecology of the Slave River Delta Using NASA Earth Observations

DEVELOP Technical Report

Final Draft – August 11th, 2022

Yuhe Chang (Project Lead)
Catherine Shea
Virgil Alfred
Ethan McIntosh

Advisors:
Dr. Cédric Fichot (Boston University) (Science Advisor)

1. Abstract

Indigenous communities around the Great Slave Lake (GSL) in Canada's Northwest Territories have observed long-term changes in water levels within the Slave River Delta (SRD), causing concern over the alteration and loss of natural and cultural resources. Changes in delta water dynamics have impeded fishing and transportation accessibility and threatened to alter important wetland ecosystems, leading to greater uncertainty in natural resources management. In partnership with the Fort Resolution Métis Government (FRMG), the Deninu K'ue First Nation (DKFN), the Akaitcho Territory Government (ATG), and Environment and Climate Change Canada (ECCC), this project provided a visual archive of water patterns and land cover in the Slave River Delta for summer months (May to October) from 1984 to 2021. We produced time series animations, maps, and charts of land cover and delta morphology changes using data from NASA's Landsat 5 Thematic Mapper (TM) and Landsat 8 Operational Land Imager (OLI) missions, augmented with other NASA-supported satellite imagery, land cover classifications, and precipitation datasets. Satellite observations confirm that changes in surface water and wetland extent in the delta tend to correlate with changes in Slave River discharge and precipitation in the drainage basin. However, we identified several water channels in the Slave River Delta and several areas of former wetland whose drying trends have persisted despite increases in precipitation and discharge from 2010 to 2020. By synthesizing various Earth observations into understandable and accessible data visualizations, the project strengthened decision-makers' overall understanding of drivers of change in the Slave River Delta.

Key Terms
Great Slave Lake, Slave River Delta, Northwest Territories, wetlands, land cover, delta, remote sensing, surface water, NASA Earth observations

2. Introduction

2.1 Background Information

The Slave River Delta is a high boreal wetland environment in Canada's Northwest Territories (NWT) nourished by sediment-rich water from the Slave River as it flows northeast from the Slave, Peace, and Athabasca basins into the Great Slave Lake. The delta, located within Akaitcho Territory and NWT Métis Nation Claimant Areas, is adjacent to the community of Fort Resolution, which is predominantly populated by First Nations and Métis peoples. The hydroecology of the delta underpins several economically and culturally important activities for local communities, including fishing, river travel, and subsistence trapping (Dagg, 2016). However, existing scientific research on long-term changes in the hydrology of the SRD is limited in scope.

Figure 1. Study area map. The RGB inset image is a composited and cloud-masked Landsat 8 OLI image of the Slave River Delta in summer 2021. The basemap of North America is from OpenStreetMap.

In order to evaluate the effects of the 1968 impoundment of the Peace River by the Bennett Dam on the shapes and sizes of water channels in the SRD, a previous study quantified changes in land and water areas using four aerial photographs of the delta taken between 1946 and 1994 (English et al., 1998). While this high-resolution photography allowed the authors to detect changes in delta morphology at a fine spatial scale, the images' temporal infrequency left a high degree of uncertainty about the processes driving the observed changes.

A recent study offered a more continuous history of hydrologic cycles in the delta through paleolimnological analysis of a sediment core from the SRD (Brock et al., 2010). The authors determined that climate-driven variability in runoff from the Slave River is likely more important in controlling flood frequencies than the regulation of the river by the Bennett Dam upstream. Another study shed light on the hydrological regimes of lakes throughout the delta through analyses of water samples collected in 2003 (Brock et al., 2007). However, both of these field-based studies examine either a single location within the delta or a single year, limiting the degree to which hydrological changes experienced by distinct water bodies in the delta can be simultaneously assessed over time.

Increasing availability of satellite-based Earth observation data allows for time series analyses of environmental change to be conducted at relatively high spatial resolutions and temporal frequencies. Optical remote sensing takes advantage of different materials' spectral properties to classify surface cover, allowing for the spatial extent of water or wetlands to be quantified. Other satellite-based technologies like altimetry can record very fine changes in surface elevation, allowing us to generate detailed time series of water levels. Using the parallel processing power of cloud computing through platforms like Google Earth Engine (GEE), decades of Earth observations can be quickly processed on a global scale. However, few studies have applied satellite-based remote sensing techniques to study the hydroecology of the SRD over time.

The primary Earth observation data underlying our analyses come from NASA's Landsat series, the longest-running satellite program for moderate-resolution optical remote sensing in existence. To ensure consistency in our time series, we considered imagery starting in 2021 and extending back to 1984, the launch year of Landsat 5, whose Thematic Mapper (TM) instrument produced images with more spectral detail and a finer (30-meter) pixel resolution than the instruments of previous Landsat missions.

2.2 Project Partners & Objectives

We partnered with Fort Resolution Métis Government (FRMG), Deninu K'ue First Nation (DKFN), Akaitcho Territory Government (ATG), and Environment and Climate Change Canada (ECCC) to analyze long-term changes in the SRD using Earth observation data. Our partners lead field-based efforts to monitor water levels, seasonal flooding patterns, fish population health, and river chemistry in the SRD. Changes in water dynamics over the past few decades have raised concerns about the ability of future generations to participate in economically and culturally important activities like boat transportation, fishing, and subsistence hunting in the delta (Dagg, 2016).

We applied a variety of Earth observation data to quantify and visualize changes in water resources within the SRD, while also exploring possible driving factors of change. We produced maps and charts visualizing the spatial extent of water within the SRD over time, focusing on the widening and narrowing of distributary channels. We also performed yearly land cover classifications of the SRD in order to quantify historical changes in the areal coverage of wetlands within the delta. Finally, we analyzed GSL water levels, Slave River flow rates, and annual precipitation within the Slave River drainage basin to determine the degree to which changes in surface water and land cover may be driven by changes in regional hydrology. Overall, we seek to demonstrate the ways in which remote sensing can enhance the existing body of literature on the SRD, while simultaneously providing compelling visualizations that enable community members of many backgrounds to effectively participate in decision-making processes to protect local water resources.

3. Methodology

3.1 Data Acquisition

3.1.1 Surface Water Data Acquisition

We used the GEE JavaScript API to access layers from the Global Surface Water (GSW) dataset, provided by the European Commission's Joint Research Centre (EC JRC), to examine changes in surface water within the SRD (Pekel et al., 2017). Within this dataset, we primarily utilized the monthly water history product, in which results from a system classifying Landsat pixels as either water or not water are reported on a monthly time step from March 1984 through December 2021 (Pekel et al., 2016). We also used the maximum water extent layer from this dataset, showing all pixels where water has been detected from 1984 to 2021. Finally, we acquired yearly "seasonality" images from GSW, in which pixels are classified as either permanent water (i.e., present for all months of the open-water season), seasonal water (i.e., present only for some months), or not water for each year in the study period.

To visualize interannual changes in delta surface water extent using an animation, we also acquired true-color satellite imagery from the Level 1, Tier 1 Top-of-atmosphere (TOA) reflectance collections of Landsat 5 and Landsat 8 (Table A1). Imagery from these two instruments is available for most of our study period, with Landsat 5 covering 1984–1999 and 2001–2011, and Landsat 8 covering 2013–2021. Landsat 5 imagery of the delta was not available for the years 2000 and 2012. We used Landsat 7 imagery to fill the gap for the year 2000, but excluded 2012 due to data gaps caused by the Scan Line Corrector failure. Our animation therefore has imagery for every year from 1984 to 2021 except for 2012. We only considered images acquired between May and October when creating our animation frames.

3.1.2 Land Cover Data Acquisition

Wetland classification images of the Slave River Delta for 2007 and 2017, created by the Arctic-Boreal Vulnerability Experiment (ABoVE) and sourced from the NASA Oak Ridge National Laboratory Distributed Active Archive Center for Biogeochemical Dynamics (ORNL DAAC), served as reference images for training our land cover classifiers (Figure B2). We ran the classifiers on annual cloud-free summer-season composites of the Slave River Delta based on Collection 2, Level 2, Tier 1 surface reflectance imagery from Landsat 5 and Landsat 8 spanning 1984–2021. Gaps in Landsat 5 data coverage at high latitudes prevented us from completing classifications for the years 2000 and 2012. For all other years in the study period (N=36), we used imagery from May through October when creating the composites in order to capture each year's ice-free season, the exact timing of which varies from year to year. In order to provide the greatest spectral differentiation between land cover classes, we considered data from bands 1-5 and 7 from Landsat 5 and bands 2-7 from Landsat 8 via GEE (Table A1). The strong absorptive tendencies of water across the electromagnetic spectrum allow our classifiers to distinguish water, wetlands, and drier land from each other.

3.1.3 Water Balance Data Acquisition

We acquired daily precipitation data, gridded at 1000 m resolution, from NASA's Daymet dataset of climatic variables to generate an annual time series of watershed precipitation. We also acquired monthly average evaporation data, with a coarser spatial resolution of 10 km on average, from the European Centre for Medium-Range Weather Forecasts' (ECMWF) Climate Reanalysis (ERA5) in order to compensate for the net precipitation that eventually flows into the Slave River. For both datasets, we used GEE to access data from 1984 to 2021 in accordance with the study period (Table A1). To accurately delineate the watershed area of the Slave River and its tributaries, we used the Canadian Digital Elevation Model (CDEM) from GEE, which provides an accurate terrain raster layer with 23-meter spatial resolution across the entire study area. We also downloaded a shapefile of regional drainage basins created by the Water Survey of Canada (WSC) and Natural Resources Canada (NRCan) in order to perform our analysis using multiple sets of watershed boundaries for robustness.

From the ECCC website, we downloaded daily estimates of Slave River discharge at station 07NB001, located in Fitzgerald, Alberta, which is the station on the Slave River geographically closest to the SRD. Finally, we acquired mean Great Slave Lake surface heights from the Global Reservoir and Lakes Monitor (G-

REALM) dataset, hosted on the United States Department of Agriculture's Foreign Agricultural Service (USDA FAS) website. These data are based on altimetric readings taken at a 10-day frequency by the Ocean Topography Experiment (TOPEX)/Poseidon and Jason-series missions operated by NASA and the Centre National D'Etudes Spatiales (CNES). We downloaded altimetric data covering October 1992 through December 2021.

3.2 Data Processing

3.2.1 Surface Water Data Processing

To create an annual time series of surface water area, we used GEE to manually delineate polygons around several of the larger Slave River Delta channels identified by partners, using the GSW maximum water extent layer as a reference so that our polygons included the fullest extent of each channel while excluding nearby lakes and ponds. We additionally drew a single larger polygon representing the outer delta, covering the land and water area bounded by the Old Steamboat Channel to the south, the main Slave River channel to the east, and the body of the lake to the north and west (Figure B5).

To create visual demonstrations of physical changes in the Slave River Delta over time, we created GIF animations of the Slave River Delta where each frame represents a single year. We created an animation of true-color imagery by masking all images for clear terrain only using Landsat's pixel quality assessment band, and then we mosaicked yearly animation frames by taking the median value for each pixel from the set of images for each year. We also animated the yearly seasonality layers from the GSW dataset clipped to the SRD from 1984 to 2020 to provide an alternative visualization focused more directly on water.

3.2.2 Land Cover Data Processing

After selecting summer-month imagery intersecting the SRD from the Landsat 5 and 8 archives covering 1984 through 2021, we assessed each image at the pixel level by filtering out saturated and cloud-related pixels and then created annual median composites. To train our land cover classifiers, we overlaid the 2008 composite from Landsat 5 and the 2017 composite from Landsat 8 with the 2007 and 2017 ABoVE classification images, respectively. We used 2008 instead of 2007 for our Landsat 5 training image, as there were not enough relatively cloudless observations of the delta during the summer of 2007 to generate a completely cloud-free training image.

We used GEE to randomly sample 140,000 points from each training image, setting a minimum distance of 10 meters between sample points in order to align them with the 10-meter resolution ABoVE reference imagery. Of the randomly sampled points, 70% (98,000) were used to train our classifiers using GEE's Random Forest Classifier algorithm, while the remaining 30% were reserved for validation. The Random Forest Classifier creates a series of decision-tree models to predict the land cover class of each randomly sampled point. The classifier makes each prediction by comparing the spectral values of each point's corresponding Landsat training pixel with each point's corresponding ABoVE reference pixel. We chose Random Forest classification over other classification methods because of its high level of accuracy and its previous usage within the ABoVE classification methodology. After training a Landsat 5 classifier and Landsat 8 classifier with the

ABoVE references using our random sample points, we applied the classifiers to the rest of our annual Landsat composites to obtain summer-month wetland classifications of the delta from 1984 through 2021.

Once our classifications of the delta were developed and tested for accuracy, we took the modified Enhanced Wetland Classification (EWC) system and further reduced the number of classes to six to develop a simpler classification scheme more aligned with the objectives of this study. Classifications of bogs, marshes, fens, and swamps were aggregated to represent an overall wetland class, and deciduous and conifer forests were consolidated into general forestry. Grouping the classes in this way yielded a 6-class scheme which allows us to be more accurate in our assessments of long-term changes in wetland extent within the SRD. Under the simplified class scheme, the 2007 and 2017 ABoVE reference images are considered by the team to be a proxy for ground truth data. These reference images had overall accuracies of 84.6% and 88.5%, respectively, under the enhanced class scheme, but their overall accuracies rise to 97.1% and 95.6%, respectively, within our simplified class scheme. Most of the errors in the enhanced ABoVE classifications are rooted in the difficulty of distinguishing between wetland types and forest types, so our method of simplifying classes eliminated most of that error.

3.2.3 Water Balance Data Processing

We tested several methods for delineating the watershed boundaries of the Slave River drainage basin. First, we generated our own watershed boundary map using the Pysheds package in Python, an open-source library designed to help with processing DEMs, particularly for hydrologic analysis. However, the watershed we created using Pysheds had large gaps over secondary drainage basins. We decided to instead rely on an existing Canadian watershed boundary shapefile from WSC, which uses a 3-level hierarchy of drainage areas. With this shapefile, we were able to easily delineate two key watersheds for our study: all land draining into the GSL through its outlet, the Mackenzie River, and all land draining into the Slave River.

We uploaded the watershed vector files into GEE to serve as the bounding areas for calculating watershed precipitation. Daymet provides daily modeled precipitation totals in millimeters. To generate an annual time series of precipitation within these watersheds, we calculated the annual total precipitation for each pixel by summing up daily values for each pixel throughout each year, and then summed up the results for all pixels in each watershed. We performed a similar process to derive annual evaporation figures from the daily ERA5 data. We derived annual net precipitation for both the GSL watershed and the Slave River watershed across the study period by subtracting evaporation from precipitation for each year. Finally, to process the G-REALM data on GSL water levels, we first filtered out invalid observations and then aggregated the original data from their 10-day frequency into yearly average lake heights for 1992 to 2021 using R. To prepare our annual time series of net watershed precipitation, Slave River discharge, and GSL water levels for analysis, we combined them into a single table.

3.3 Data Analysis

3.3.1 Surface Water Data Analysis

Using GEE, we calculated the area in square kilometers within each channel polygon that was classified as water, not water, or no data within the GSW monthly water history layers from 1984 to 2020. To aggregate our monthly surface water area calculations to an annual time step, we took averages for each year, excluding any monthly observations where more than 5% of the pixels in a polygon were classified as no data. The authors of a recent study of changes in global lake and reservoir surface water area used the same 5% threshold in order to limit the level of uncertainty for their calculations of water surface area (Busker et al., 2019). In the context of the GSL, applying this threshold filtered out almost all non-summer observations, where ice and snow cover resulted in many no-data pixels. Each yearly data point can thus be thought of as an average summer-month surface water area for that year.

To analyze our time series data on the yearly surface water areas of individual waterways in the SRD, we created line charts plotting each channel's surface water area over time relative to 1984. One chart depicts the area of surface water, in square kilometers, gained or lost by each channel relative to its 1984 water area. Another chart reports these changes in surface water area as percentages of each channel’s water surface area in 1984 (Figure 4). We also considered changes in the surface water area of the entire outer delta by summing the yearly surface water area totals for all channels and plotting the data on a chart (Figure B1).

3.3.2 Land Cover Data Analysis

Following the classification of Landsat 5 and Landsat 8 imagery, we created a confusion matrix in GEE to test the training and validation accuracies of the classifiers. Of the original 140,000 random sample points, 30% (42,000) were reserved as validation pixels to undergo a classification of their own, and then be compared to initial results. We maximized the number of sample points according to the processing capabilities of GEE and maintained a training to testing ratio of 70:30. We tested an 80:20 ratio for the Landsat 5 classifier in alignment with ABoVE’s Random Forest process but found that this ratio did not meaningfully improve our classification accuracies. We therefore opted to use the more robust 70:30 ratio.

To analyze wetland extent over time, we calculated the area of land occupied by each land cover class by extracting pixel counts for each year in the study period under both the enhanced and simplified classifiers. We performed some additional filtering on the results in order to generate a more accurate time series of wetland extent in the SRD (Figure B3). To account for variation in the availability of cloud-free scenes for certain years in the wetland time series, we devised a metric which we will refer to as the “cloud-free score” for each annual composite. We defined this metric as the number of scenes’ worth of cloud-free pixels that went into a given annual composite image, and we considered composites with higher cloud-free scores to be more reliable for classification than composites with lower cloud-free scores. To calculate each cloud-free score, we added up the fractional Landsat cloud scores of all summer-month scenes that were acquired for each year’s composite image and subtracted that number (representing the number of images covered by clouds) from the total number of scenes collected for a given composite.

The average cloud-free score of our 36 classified images was 23.8, with a standard deviation of 4.2. We filtered out observations with a cloud-free score below 19.6 (i.e., at least one standard deviation below the average cloud-free score). Applying this filter removed 6 observations out of the 36 years in our time series (Table A2). As an additional step to address high year-to-year variability in the wetland area time series, we also filtered out two years, 1994 and 2006, for which the calculated total wetland area was more than 2 standard deviations above or below the average of the previous and following two years of data.

Based on our time series of wetland surface areas in the SRD, we created tri-color maps symbolizing three types of land cover change: wetlands to forest, wetlands to shrubland, and all other classes to wetlands. Using geospatial packages in Python, we created these change images for three intervals of time: 1984 to 2021 (overall change within the study period), 2005 to 2010 (an example of a drying period), and 2010 to 2020 (an example of a wetting period).

3.3.3 Water Balance Data Analysis

In order to assess relationships between changes in surface water area in the SRD, Slave River watershed precipitation, changes in GSL water levels, and Slave River flow rates, we first normalized the data we acquired for these variables by applying a Min-Max Scaling function (Equation 1).

$$X' = \frac{X - X_{min}}{X_{max} - X_{min}}$$

The normalized data fall between 0 and 1 and are unitless, which makes them more statistically comparable. We then calculated Pearson correlation coefficients, R-squared values, and corresponding p-values based on normalized datasets to assess statistical significance. These statistical analyses were performed using our annual time series numbers for each variable from 1984 to 2021 (N = 38), except for GSL water levels, which were only available for 1993 to 2021 (N = 29). The annual change of water levels is defined as the water level of the study year subtracted by the water level of last year; we obtained 28 values of annual water level change for 1994 to 2020.

We also investigated the spatial distribution of areas in the SRD that experienced a statistically significant trend in precipitation volume change from 2010 through 2020 by applying the Mann-Kendall test, which is a non-parametric method for identifying statistically significant trends in time series data. We applied this test to the annual precipitation data for each pixel in the watershed area, setting the Alpha parameter to 0.1.

4. Results & Discussion

4.1 Analysis of Results

4.1.1 Surface Water Results

Every channel except for the main body of the Slave River appears to have shrunk slightly in terms of surface water area, although 2020 saw a few channels regain some surface water (Figure 2). The Old Steamboat Channel shrunk by 0.6 square kilometers, which marks more surface water loss in absolute terms than any other

channel. However, other channels like the East Channel, Middle Channel West, and Middle Channel South experienced almost 100% loss of surface water areas relative to 1984 during at least one year in the study period.

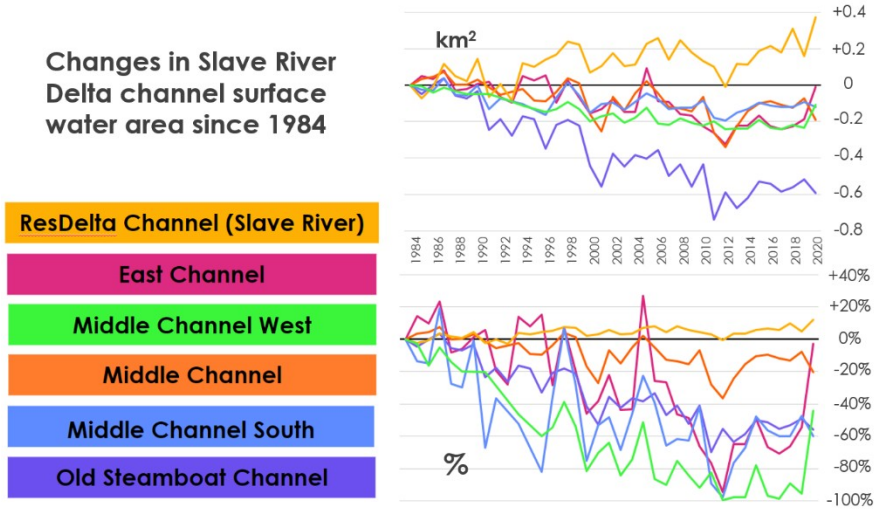

Figure 2. Changes in the surface water area of individual waterways in the outer Slave River Delta, expressed in square kilometers of water relative to 1984 (top) and in percent water area relative to 1984 (bottom).

The surface water areas of all the channels tend to rise and fall together, with local peaks in most channels around 1997 and 2005 and local lows around 2001 and 2010. However, the long-term trends of the channels are divergent, with most channels losing some surface water area while the ResDelta Channel, the main body of the Slave River, has expanded somewhat. A previous study of delta channel morphology based on aerial photography suggested that a greater portion of the water coming down the Slave River between the 1940s and the 1990s was flowing through the ResDelta Channel, the main body of the Slave River, rather than through other distributary channels in the outer delta, possibly as a result of sediment deposition patterns (English et al., 1998). Our results confirm that this divergent trend has continued steadily through 2021 and, as we discuss in section 4.1.3, distributary channel shrinkage seems to be independent of long-term overall trends in the amount of water flowing through the Slave River. We would therefore tentatively attribute the long-term loss of surface water in channels like the Old Steamboat to sediment deposition patterns narrowing their entrances, diverting water into the main ResDelta Channel.

4.1.2 Land Cover Results

Our Landsat 5 enhanced classification had a 98.6% training accuracy and a 60.7% validation accuracy (Table A3), and our Landsat 8 enhanced wetland classification had a 98.6% training accuracy and a 58.8% validation accuracy (Table A5). These accuracies were expectedly low, since our classifications (Figure B3) were based entirely on spectral data from Landsat imagery, unlike the ABoVE references (Figure B2) that were created using data from additional instruments and field work. However, re-computing the enhanced validation error matrices into our simplified class scheme yielded overall validation accuracies of 83.8% for Landsat 8 (Table A4) and 83.4% for Landsat 5 (Table A6). Furthermore, the user accuracies for the simplified wetland class, which became the focus of our study, were 85.2%

for the Landsat 5 classifier and 86.2% for the Landsat 8 classifier. These results suggest that our satellite image classifications can offer broadly reliable estimates of wetland extent over time, albeit with limited accuracy.

After performing classifications on all years in the study period, calculating the area covered by each land cover class for each year, and filtering out cloudier years and outliers (as described in section 3.3.2), we found that the total area classified as wetland in the SRD appears to follow a multi-year cyclical trend, with alternating wetting and drying periods (Figure 3). Total wetland-classified surface area decreased from roughly 2,500 km^2 in 1993 to roughly 1,900 km^2 in 1999 before rebounding to about 2,600 km^2 in 2005. By 2010, wetland-classified area decreased to around 2,100 km^2 before rising again to almost 2,500 km^2 in 2020.

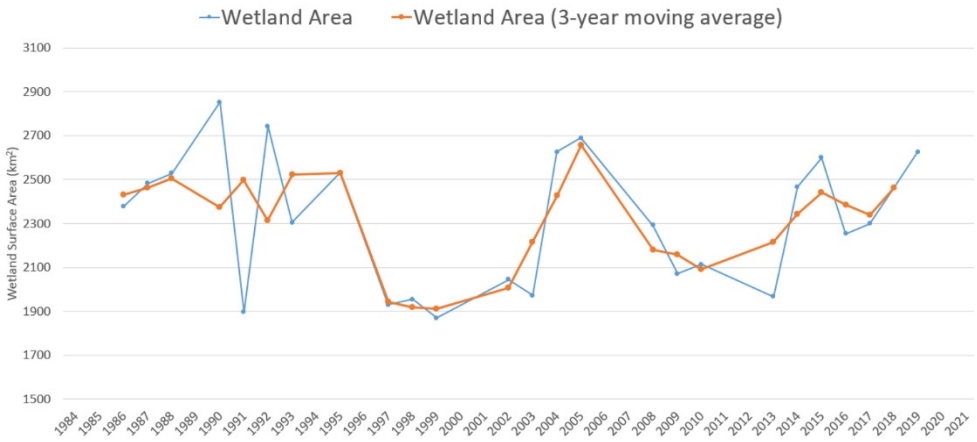

Figure 3. Surface area in the Slave River Delta classified as wetlands, 1984–2021

The timing of high and low points in our wetland extent time series generally matches the timing of highs and lows in outer delta channel surface water areas (Figure 2). For example, the mid-1990s are a wetter period in our wetland time series, which is consistent with the results of a paleolimnological analysis of the SRD that identified the mid-1990s as a time of increased flood frequency (Brock et al., 2010). However, the limited accuracies of our classifiers preclude any strong conclusions about what these cycles represent in hydrological or ecological terms. For areas that changed from one class to another, it is difficult to determine with a high degree of certainty whether they are undergoing longer-term ecosystem changes or simply experiencing the normal cycles between wetter and drier periods that are typical of wetland habitats. However, we can partially reduce these ambiguities by analyzing our results in a spatially explicit way.

To visualize the spatial distribution of land in the SRD that experienced wetting and drying trends, we created maps of pixel-level changes in simplified classification results that occurred during a drying period (2005–2010), a wetting period (2010–2020), and over the full study period (1984–2021) (Figure 4). Many of the areas where class changes occurred from 2005–2010 and from 2010–2020 are close to the body of the Slave River. One possible explanation for this pattern is that our classification results are sensitive to interannual cycles in the discharge and flood frequency of the Slave River, which would affect areas closest to the river the most. However, a previous study comparing the hydrological drivers of

multiple lakes in the SRD in 2003 found that almost all of the lakes whose water balances are dominated by flood events were near the mouth of the Slave River, rather than the middle and upper parts of the delta, where the hydrology of most lakes was primarily controlled by evaporation (Brock et al., 2007). If flood frequency were the only factor explaining the spatial distribution of the land cover changes detected by our classifications, we would therefore expect more concentrated greens and blues to be present near the mouth of the river. Instead, our maps show the most concentrated areas of class change along the middle and upper portions of the river.

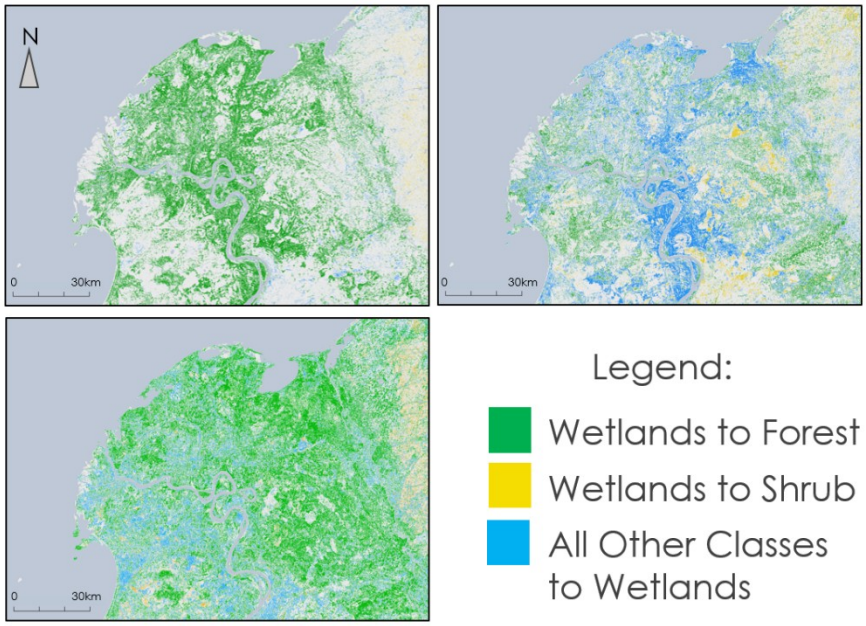

Figure 4. Simplified wetland class changes between 2005 and 2010 (top left), 2010 and 2020 (top right), and 1984 and 2021 (bottom left).

In order to try and address our project partners' particular concern about longer-term ecosystem changes in the SRD, we sought to identify areas where changes from wetlands to drier classes seemed to be occurring independently of the overall wetting and drying trends. During the drying period from 2005 to 2010, very few pixels changed from other classes to wetlands. However, large areas that were classified as wetlands in 2010, particularly in the delta's eastern portion, were reclassified as forest or shrubs in 2020, despite the overall wetting trend during that period. Furthermore, although the total area classified as wetlands was roughly equal at both the start and end of our study period, the spatial distribution of wetlands has drastically shifted away from the eastern portion of the delta. These patterns suggest that among areas within the delta, the eastern portion seems most likely to be experiencing longer term ecosystem shifts rather than simple cycling between wetter and drier patterns in an otherwise-stable wetland ecosystem. However, these results cannot be fully confirmed due to the limited availability of ground-truth data to assess the accuracy of our classifications distinguishing wetlands from other classes over the full study period.

4.1.3 Water Balance Results

One factor that may affect the changing distribution of wetlands over time is precipitation. The Mann-Kendall test results for the entire Slave River drainage basin show that a large portion of the watershed experienced a significant increase in precipitation, most of which was near the body of the Slave River. Roughly a third of the surface area of the delta itself also experienced a consistent increase in precipitation during that decade. Areas of positive precipitation trends are mostly in the northeastern and southern parts of the delta, generally coinciding with the spatial pattern of wetland increase in the same period (Figure 5).

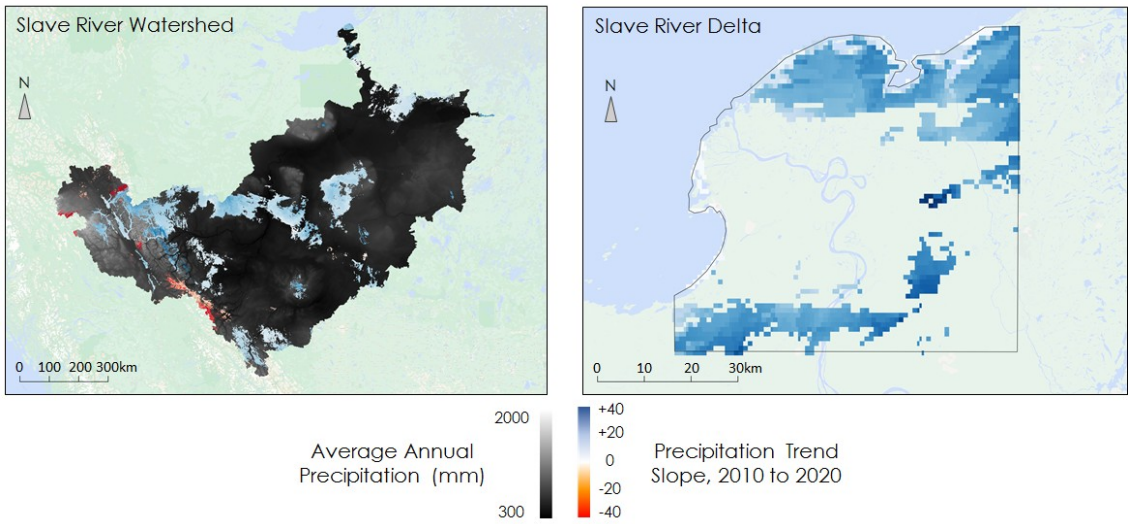

Figure 5. Precipitation trends from 2010 through 2020 within the Slave River drainage basin (left) and the SRD (right). Trend results for the drainage basin are overlaid on a layer showing the spatial distribution of average annual precipitation.

More generally, we observed Slave River watershed precipitation to be tightly associated with both river discharge and Great Slave Lake water levels. Discharge and changes in water levels have their high and low points during the same years as precipitation (Figure 6). Several of these high and low points also correspond with the timing of drying and wetting periods in delta land cover, as discussed in the previous section. However, there is sometimes a time lag between precipitation changes and water level changes.

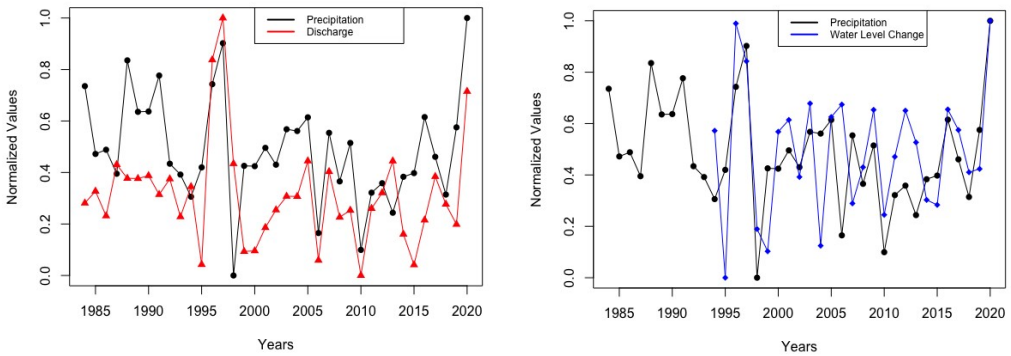

Figure 6. Comparison of normalized annual values for Slave River drainage basin precipitation vs. Slave River discharge (left) and Slave River drainage basin precipitation vs. average Great Slave Lake water levels (right).

Linear regression analysis supported our judgement of the strength of precipitation as a predictor of discharge and water levels. The results of linear regression between annual precipitation over the Slave River drainage basin and the annual discharge of the river demonstrate a fairly strong relationship (Figure B4). The slope is 0.706 with a p-value of 0.00015. The R-squared reaches 0.33, which confirms previous findings that Slave River watershed precipitation is the dominant factor in the overall water balance of the Great Slave Lake (Gibson et al., 2006). We achieved similar results for precipitation and water level changes. The slope for these two variables is 0.538 with a p-value of 0.00019. The corresponding R-squared also revealed the strong influence the precipitation has on the lake water levels, with the actual number to be 0.44. For robustness, we also ran these regressions using net precipitation (total precipitation minus evaporation) as our regressor instead of total precipitation, and we continued to find statistically significant ($p < 0.05$) results for both relationships, albeit with slightly lower R-squared values of 0.32 for discharge and 0.31 for water levels.

The results of linear regression between annual precipitation and annual surface water area changes, on the other hand, were not statistically significant. The corresponding slope was 0.192, with a p-value of 0.30000. The weakness of precipitation as a predictor of surface water extent changes suggests that precipitation is not among the primary causes of the shrinkage of channels in the delta. This is what we expected, because precipitation does not map 1-to-1 onto the kinds of flood events that fill up channels during the summer months, which are also influenced by other factors, such as winter ice jam patterns (Das et al., 2015). Considering the strong correlation between precipitation and discharge, sediment deposition might be the primary contributor to the consistent channel shrinkage. This hypothesis is backed up by the fact that the only channel that did not show a significant decrease in its surface water extent was the main channel of Slave River, through which the majority of the discharge flows into the lake. The change of the surface water extent of this channel matched the changing pattern of the discharge decently, which fluctuated throughout the study period but did not consistently decrease. The apparent lack of water in other sub-channels wasn’t due to the limited water input, but more likely the blockage of the water entrances by deposited sediment.

4.2 Future Work

Our results and limitations in applying satellite-based Earth observations to study long-term hydroecological changes in the Slave River Delta point to both the potential for future applications of remote sensing in the region and the importance of field-based reference data. Other satellite-based data like c-band radar could be used to delineate surface water and help classify land cover during seasons when high cloud cover reduces the utility of visible to infrared wavelength imagery, thereby allowing researchers to cross-validate their results and reduce levels of uncertainty. Other technologies like high-resolution drone imagery could provide greater precision in both our imagery and in the quantitative data on areal coverage of water and wetlands. However, additional field surveys of habitat, biomass accumulation, and hydrological variables like water levels and discharge within the SRD itself would be critical in helping refine or alter our conclusions

about changes in the delta ecosystem and open up new questions to guide the acquisition of remotely sensed data.

Our partners could benefit from increased accessibility and flexibility in exploring the data and insights produced by analyses of remotely sensed data. Being able to present our data through a web-based graphical user interface would allow partners and community members of varying levels of technical expertise to access data more easily and apply their own parameters to visualize changes according to custom time frames or color schemes. Such platforms have the potential to enhance broader public engagement and advocacy relating to important environmental changes.

Finally, our research and our discussions with partners point to additional topics of research related to water dynamics that are worth further investigation in order to address community concerns and elevate the state of knowledge on environmental changes in the SRD. To better understand the dynamics of channel water shifting in the SRD, we believe that we could benefit from a closer analysis of interannual and seasonal changes in sediment deposition, with specific focus on the early 2000s, when there was an especially pronounced change in channel surface water extents and topography. Seasonal ice dynamics, which are an important factor in controlling river discharge, could be investigated with radar imagery and other Earth observation data as well as ground-based research. Having a stronger sense of trends, or lack-of-trends, between weather events, melting periods, and channel structure could better direct stakeholder decision making regarding water transportation in the delta. Finally, community concerns about muskrat populations in the delta could be addressed by future field-based research on muskrat populations, as well as by more field-based work on ecological changes in key areas of the delta.

5. Conclusions

We've shown that satellite-based Earth observations can identify long-term environmental changes that speak well to community concerns about the future of water transportation and wetland habitats in the Slave River Delta. Through our research, we've determined that many waterways in the outer SRD have been steadily losing surface water, while the main river channel has expanded. Our analysis of these changes in relation to watershed precipitation, river discharge, and lake water levels suggests that long term channel shrinkage may be primarily driven by sedimentation blocking off sections of channels, rather than just being a result of changes in overall precipitation and discharge.

We also found that land cover in the delta seems to experience cycles between wetter and drier vegetation, broadly correlating with precipitation trends. Although limited historical ground-truth data prevents us from distinguishing between normal wetland hydrological cycling and more permanent habitat change with a high degree of certainty, we were able to apply spatial methods to identify areas in the eastern portion of the delta whose drying patterns seem independent of precipitation trends. These areas may warrant further investigation and attention in future habitat preservation efforts and in ongoing research on the future of wetland ecosystems in the SRD.

Satellite-based Earth observations, in addition to providing longitudinal and spatially rich perspectives for scientific research, have rich potential in informing environmental policy, education, and advocacy. Our partners working in Fort Resolution can apply the information we gathered on surface water and land cover changes to target field-based interventions for mitigating channel shrinkage and preserving wetland habitat. Satellite-derived imagery of surface water and land cover also illustrates environmental changes to residents more broadly, thereby animating communities' ongoing environmental advocacy efforts. By tailoring our research according to the community concerns of partners living and working in the Slave River Delta, we hope to provide examples of ways in which analyses of Earth observation data can support efforts to address pressing environmental challenges more broadly.

6. Acknowledgments

We wish to acknowledge our partners from the FRMG (Shawn McKay), the DKFN (Minnie Whimp and Kathleen Fordy), the ATG (Diane Giroux and Mike Tollis), and the ECCC (Marlene Evans) for their valuable suggestions throughout the project. We are also grateful for the advice and guidance on remote sensing data and methods we received from our science advisor, Dr. Cédric Fichot, throughout the term. Finally, we want to thank the Massachusetts – Boston Fellows of the NASA DEVELOP program, Tyler Pantle and Celeste Gambino, for their helpful feedback on every aspect of our project and for their excellent leadership.

Maps throughout this work were created using QGIS Geographic Information System software, published by the Open Source Geospatial Foundation Project (http://qgis.osgeo.org).

This material is based upon work supported by NASA through contract NNL16AA05C.

7. Glossary

Altimetry – In general, refers to the measurement of heights. Satellite-based altimeters use radar pulses to accurately measure surface heights by tracking the time each pulse takes to return to the instrument.
Boreal – A sub-arctic climate characterized by short mild summers, occurring in latitudes between 50 and 70 degrees North.
Channel morphology – The shapes of river channels and how they change over time.
Composite image – An image whose pixels are stitched together from several images covering the same spatial area. The images being stitched together may come from different dates, viewing angles, or sensors.

Confusion matrix – A table used to measure the accuracy between classification predictions and true values.
Discharge/flow – The rate at which a volume of water passes by a given cross-section of a river or stream.
Distributary channel – Water that branches off and flows away from the main body of a river.
Drainage basin/watershed – An area of land where all precipitation eventually flows into a common water outlet.
Hydroecology – The study of interactions between hydrology and living ecosystems, such as wetland habitat.
Hydrology – The study of the movement and distribution of water at or near the Earth's surface.
Median image – An image in which each pixel value is taken from the median of that pixel's non-null values across a collection of spatially overlapping images.
Mosaicking – The process of combining multiple images from nearby spatial areas into a single larger image
Random Forest Classifier – A method of classification in which a multitude of randomly generated decision trees are used to identify the discrete class or category to which an observation belongs, and then a final classification is determined by taking a majority vote of the decision trees.
Reflectance – The portion of all light shining upon a material that the material reflects.
Remote sensing – Techniques and processes for detecting the physical qualities of an area by measuring the radiation reflected and emitted by that area from a distance, usually from satellites or aircraft.
Seasonality – The quality of an environmental pattern of change to occur along a predictable time scale.
Spatial Resolution – The smallest size of an area for which a given sensor can distinguish that area from its surroundings. Spatial resolution for imagery is often reported in terms of pixel size, or the geographic distance covered by the length of one image pixel.
Spectral differentiation – Using multiple recorded energy signatures along the electromagnetic spectrum to differentiate features in remote sensing imagery.
Temporal Resolution – The unit of time between observations in a dataset of repeated measurements. This may also be referred to as the return frequency or observation frequency.
Water Balance – A ratio between added quantities and lost quantities within a body of water, considering precipitation, evaporation, river discharge, and other trends.

8. References

Brock, B. E., Martin, M. E., Mongeon, C. L., Sokal, M. A., Wesche, S. D., Armitage, D., Wolfe, B. B., Hall, R. I., & Edwards, T. W. D. (2010). Flood frequency variability during the past 80 years in the Slave River Delta, NWT, as determined from multi-proxy paleolimnological analysis. *Canadian Water Resources Journal*, *35*(3), 281–300. https://doi.org/10.4296/cwrj3503281

Brock, B. E., Wolfe, B. B., & Edwards, T. W. D. (2007). Characterizing the hydrology of shallow floodplain lakes in the Slave River Delta, NWT, Canada, using water isotope tracers. *Arctic, Antarctic, and Alpine Research*, *39*(3), 388–401. https://doi.org/10.1657/1523-0430(06-026)[BROCK]2.0.CO;2

Busker, T., de Roo, A., Gelati, E., Schwatke, C., Adamovic, M., Bisselink, B., Pekel, J.-F., & Cottam, A. (2019). A global lake and reservoir volume analysis using a surface water dataset and satellite altimetry. *Hydrology and Earth System Sciences*, *23*(2), 669–690. https://doi.org/10.5194/hess-23-669-2019

Dagg, J. (2016). *State of the Knowledge of the Slave River and Slave River Delta: A Component of the Vulnerability Assessment of the Slave River and Delta.* The Pembina Institute, with input and updates by the Government of Northwest Territories. https://www.nwtwaterstewardship.ca/sites/water/files/resources/final_april16_final_slave_river_state_of_the_knowledge_report.pdf

Das, A., Sagin, J., Van der Sanden, J., Evans, E., McKay, H., & Lindenschmidt, K.-E. (2015). Monitoring the freeze-up and ice cover progression of the Slave River. *Canadian Journal of Civil Engineering*, *42*(9), 609–621. https://doi.org/10.1139/cjce-2014-0286

ECCC (n.d.). *Historical Hydrometric Data: Slave River at Fitzgerald (Alberta)*. Retrieved from: https://wateroffice.ec.gc.ca/report/historical_e.html?stn=07NB001

ECMWF (n.d.). *Climate Reanalysis version 5 (ERA5)*. https://doi.org/10.24381/cds.adbb2d47

English, M. C., Hill, R. B., Stone, M. A., & Ormson, R. (1997). Geomorphological and botanical change on the Outer Slave River Delta, NWT, before and after impoundment of the Peace River. *Hydrological Processes*, *11*(13), 1707–1724. https://doi.org/10.1002/(SICI)1099-1085(19971030)11:13<1707::AID-HYP600>3.0.CO;2-O

French, N. H. F., Graham, J. A., Vander Bilt, D. J. L., Jenkins, L. K., Battaglia, M. J., & Bourgeau-Chavez, L. L. (2022). *ABoVE: Wetland Type, Slave River and*

Peace-Athabasca Deltas, Canada, 2007 and 2017 [Data set]. ORNL DAAC, Oak Ridge, Tennessee, USA. https://doi.org/10.3334/ORNLDAAC/1947

Gibson, J. J., Prowse, T. D., & Peters, D. L. (2006). Hydroclimatic controls on water balance and water level variability in Great Slave Lake. *Hydrological Processes*, *20*(19), 4155–4172. https://doi.org/10.1002/hyp.6424

Pekel, J.-F., Cottam, A., Gorelick, N., & Belward, A. S. (2016). High-resolution mapping of global surface water and its long-term changes. *Nature*, *540*(7633), 418–422. https://doi.org/10.1038/nature20584

Pekel, J. F., Cottam, A., Gorelick, N., & Belward, A. (2017). *Global Surface Water Explorer dataset* [Data set]. European Commission, Joint Research Centre (JRC). http://data.europa.eu/89h/jrc-gswe-global-surface-water-explorer-v1

Thornton, M. M., Shrestha, R., Wei, Y., Thornton, P. E., Kao, S., & Wilson, B. E. (2020). *Daymet: Daily Surface Weather Data on a 1-km Grid for North America* (Version 4) [Data set]. ORNL DAAC, Oak Ridge, Tennessee, USA. https://doi.org/10.3334/ORNLDAAC/1840

USDA/NASA G-REALM program (n.d.). *G-REALM: Great Slave Lake.* Retrieved from: https://ipad.fas.usda.gov/cropexplorer/global_reservoir/gr_regional_chart.aspx?regionid=can&reservoir_name=Great_Slave&lakeid=000420

U.S. Geological Survey Earth Resources Observation and Science Center. (2012). *Landsat 4-5 TM Level-2 Surface Reflectance (SR)* [Data set]. U.S. Geological Survey. https://doi.org/10.5066/P918ROHC

U.S. Geological Survey Earth Resources Observation and Science Center. (2012). *Landsat 4-5 TM Level-1 Top of Atmosphere (TOA) Reflectance* [Data set]. U.S. Geological Survey. https://doi.org/10.5066/F7N015TQ

U.S. Geological Survey Earth Resources Observation and Science Center. (2022). *Landsat 7 ETM+ Level-1 Top of Atmosphere (TOA) Reflectance* [Data set]. U.S. Geological Survey. https://doi.org/10.5066/F7WH2P8G

U.S. Geological Survey Earth Resources Observations and Science Center. (2022). *Landsat 8 OLI/TIRS Level-2 Surface Reflectance (SR)* [Data set]. U.S. Geological Survey. https://doi.org/10.5066/F71835S6

U.S. Geological Survey Earth Resources Observations and Science Center. (2022). *Landsat 8 OLI/TIRS Level-1 Top of Atmosphere (TOA) Reflectance* [Data set]. U.S. Geological Survey. https://doi.org/10.5066/F71835S6

Appendix A

Table A1:
Information on Acquired Datasets

Name	Source	Product Type/Level	Spatial Resolution	Date Range	Frequency
Landsat 5 Thematic Mapper (TM)	NASA	Level 1, Collection 1, Tier 1 top-of-atmosphere reflectance (for animation); Level 2, Collection 2, Tier 1 (for classification)	30m	1984-2013	16 days
Landsat 7 Enhanced Thematic Mapper Plus (ETM+)	NASA	Level 1, Collection 1, Tier 1 top-of-atmosphere reflectance (for animation)	30m	2000	16 days
Landsat 8 Operational Land Imager (OLI)	NASA	Level 1, Collection 1, Tier 1 top-of-atmosphere reflectance (for animation); Level 2, Collection 2, Tier 1 surface reflectance (for classification)	30m	2013-2021	16 days
Arctic-Boreal Vulnerability Experiment (ABoVE)	NASA, ORNL-DAAC	Land Cover Classification Imagery	10m	2007, 2017	Discrete
Global Surface Water (GSW)	EC JRC	Landsat pixels classified as water / no water / no data	30m	1984-2020	Monthly; yearly
Daymet V4: Daily Surface Weather and Climatological Summaries	NASA, ORNL-DAAC	Gridded estimates of daily precipitation, measured in meters of liquid water equivalent.	1000m	1984-2021	Daily
Canadian Digital Elevation Model (CDEM)	NRCan	Collection of ground or reflective surface elevations	~ 23m	pubd. 2013	Discrete
Watersheds in Canada	WSC, NRCan	Feature layer depicting the watershed boundaries of Canada.	N/A	1927-2015	Discrete

Global Reservoir and Lake Monitor (G-REALM)	USDA FAS, NASA, CNES	Mean lake surface water height (meters) above sea level	N/A	1992-2021	10 days
ERA5-Land Monthly Averaged - ECMWF Climate Reanalysis	ECMWF	Monthly averaged evaporation estimation (meters in liquid water equivalent)	11132m	1981-present	Monthly
Historical Hydrometric Data	ECCC	Daily estimates of river discharge (m^3/s)	N/A	1984-2021	Daily

Table A2:
Information used to filter yearly wetland extent results (years that were filtered out are highlighted)

Year	Num. of Landsat scenes acquired	Calculated wetland area was an outlier	Cloud-free score	Year	Num. of Landsat scenes acquired	Calculated wetland area was an outlier	Cloud-free score
1984	30	false	18.19	**2003**	42	false	25.32
1985	35	false	20.48	**2004**	44	false	27.17
1986	36	false	20.11	**2005**	49	false	25.89
1987	41	false	26.86	**2006**	49	true	22.71
1988	40	false	25.09	**2007**	41	false	18.33
1989	32	false	19.03	**2008**	44	false	28.85
1990	37	false	22.83	**2009**	46	false	27.29
1991	46	false	22.78	**2010**	43	false	23.55
1992	40	false	27.04	**2011**	36	false	18.15
1993	43	false	24.19	**2013**	43	false	23.12
199	40	true	28.67	**201**	49	false	23.96

4				4			
1995	45	false	22.58	2015	53	false	25.29
1996	42	false	19.47	2016	53	false	29.06
1997	35	false	20.75	2017	54	false	32.91
1998	38	false	24.84	2018	55	false	27.79
1999	41	false	21.01	2019	50	false	24.42
2001	25	false	10.66	2020	44	false	24.67
2002	49	false	28.09	2021	43	false	25.44

Table A3:
Landsat 5 enhanced wetland classification error matrix

Class Names	Water	Floating Aquatic Vegetation	Emergent Marsh	Meadow Marsh	Open Fen	Shrubby Fen	Treed Fen	Shrubby Bog	Treed Bog	Shrub Swamp	Hardwood Swamp	Conifer Swamp	Upland Conifer Forest	Upland Deciduous Forest	Upland Shrub	Barren, Stone	User Totals	User Accuracies
Water	7131	196	38	0	2	0	0	0	0	1	0	1	0	0	0	1	7370	96.76%
Floating Aquatic Vegetation	42	165	104	4	7	1	2	0	0	5	0	30	13	1	0	0	374	44.12%
Emergent Marsh	22	130	500	46	46	8	67	0	14	102	12	93	32	6	7	2	1087	46.00%
Meadow Marsh	0	5	59	511	185	91	41	0	42	249	11	3	1	16	26	11	1251	40.85%
Open Fen	1	8	27	100	146	19	19	0	7	87	3	6	0	4	7	5	439	33.26%
Shrubby Fen	0	3	23	61	45	142	43	0	19	185	0	10	2	11	20	2	566	25.09%
Treed Fen	0	14	107	78	57	196	1084	0	210	484	9	409	203	60	11	3	2925	37.06%
Shrubby Bog	0	0	0	0	0	0	0	0	0	0	0	0	0	0	0	0	0	N/A
Treed Bog	0	3	3	1	3	7	33	0	30	35	2	17	14	10	2	0	160	18.75%
Shrub Swamp	2	40	267	536	298	613	749	0	384	3588	96	222	235	708	130	9	7877	45.55%
Hardwood Swamp	0	1	15	5	1	0	1	0	1	19	26	2	4	12	0	0	87	29.89%
Conifer Swamp	0	76	143	21	16	33	404	0	83	156	16	1799	764	16	10	0	3537	50.86%
Upland Conifer Forest	0	19	51	20	7	7	113	0	50	235	71	833	3164	296	19	1	4886	64.76%
Upland Deciduous Forest	0	5	9	17	4	2	39	0	29	410	141	19	260	1990	5	1	2931	67.89%
Upland Shrub	0	0	7	19	8	24	4	0	16	60	0	2	1	2	486	125	754	64.46%
Barren, Stone	2	2	0	0	1	0	2	0	0	3	0	0	0	0	128	310	448	69.20%
Producer Totals	7200	667	1353	1419	826	1143	2601	0	885	5619	387	3446	4693	3132	851	470	**Overall accuracy:**	
Producer Accuracies	99.04%	24.74%	36.95%	36.01%	17.68%	12.42%	41.68%	N/A	3.39%	63.85%	6.72%	52.21%	67.42%	63.54%	57.11%	65.96%		**60.74%**

Table A4:
Landsat 5 simplified wetland classification error matrix

Class Names	Water	Floating Aquatic Vegetation	Wetlands	Forest	Shrub	Barren, Stone	User Totals	User Accuracies
Water	7131	196	42	0	0	1	7370	96.76%
Floating Aquatic Vegetation	42	165	153	14	0	0	374	44.12%
Wetlands	25	280	15281	2098	213	32	17929	85.23%
Forest	0	24	2057	5710	24	2	7817	73.05%
Shrub	0	0	140	3	486	125	754	64.46%
Barren, Stone	2	2	6	0	128	310	448	69.20%
Producer Totals	7200	667	17679	7825	851	470	**Overall accuracy:**	
Producer Accuracies	99.04%	24.74%	86.44%	72.97%	57.11%	65.96%		**83.83%**

Table A5:
Landsat 8 enhanced wetland classification error matrix

Class Names	Water	Floating Aquatic Vegetation	Emergent Marsh	Meadow Marsh	Open Fen	Shrubby Fen	Treed Fen	Shrubby Bog	Treed Bog	Shrub Swamp	Hardwood Swamp	Conifer Swamp	Upland Conifer Forest	Upland Deciduous Forest	Upland Shrub	Barren, Stone	User Totals	User Accuracies
Water	4507	33	38	0	0	0	0	0	0	1	2	3	3	0	0	0	4587	98.26%
Floating Aquatic Vegetation	22	84	41	27	5	6	2	0	11	14	0	16	3	2	2	0	235	35.74%
Emergent Marsh	49	96	731	33	27	90	71	0	14	147	9	155	20	10	6	2	1460	50.07%
Meadow Marsh	0	35	20	278	75	76	46	0	62	55	0	4	0	1	1	6	659	42.19%
Open Fen	0	7	4	39	103	20	5	0	15	10	0	0	0	0	0	15	218	47.25%
Shrubby Fen	0	32	121	151	68	573	207	0	55	298	3	49	1	1	32	1	1592	35.99%
Treed Fen	0	9	129	31	9	240	1014	0	64	517	2	452	19	12	32	0	2530	40.08%
Shrubby Bog	0	0	0	0	0	0	0	0	0	0	0	0	0	0	0	0	0	N/A
Treed Bog	0	38	5	87	29	80	32	0	637	203	1	36	0	37	72	6	1263	50.44%
Shrub Swamp	0	85	155	97	46	362	523	0	297	2354	119	519	40	463	150	7	5217	45.12%
Hardwood Swamp	0	0	1	0	0	0	1	0	0	34	40	1	1	33	0	0	111	36.04%
Conifer Swamp	12	45	131	4	9	58	587	0	136	399	5	2642	917	187	36	0	5168	51.12%
Upland Conifer Forest	2	7	29	1	0	4	20	0	22	77	13	910	2603	347	0	0	4035	64.51%
Upland Deciduous Forest	1	19	35	3	0	5	17	0	43	489	189	253	292	2280	6	0	3632	62.78%
Upland Shrub	0	1	13	3	6	17	24	0	57	136	0	50	0	1	897	85	1290	69.53%
Barren, Stone	0	0	1	0	3	0	0	0	5	3	0	0	0	0	81	327	420	77.86%
Producer Totals	4593	491	1454	754	380	1531	2549	0	1418	4737	383	5090	3899	3374	1315	449	**Overall accuracy:**	
Producer Accuracies	98.13%	17.11%	50.28%	36.87%	27.11%	37.43%	39.78%	N/A	44.92%	49.69%	10.44%	51.91%	66.76%	67.58%	68.21%	72.83%		**58.83%**

Table A6:

Landsat 8 simplified wetland classification error matrix

Class Names	Water	Floating Aquatic Vegetation	Wetlands	Forest	Shrub	Barren, Stone	User Totals	User Accuracies
Water	4507	33	44	3	0	0	4587	98.26%
Floating Aquatic Vegetation	22	84	122	5	2	0	235	35.74%
Wetlands	61	347	15702	1742	329	37	18218	86.19%
Forest	3	26	2110	5522	6	0	7667	72.02%
Shrub	0	1	306	1	897	85	1290	69.53%
Barren, Stone	0	0	12	0	81	327	420	77.86%
Producer Totals	4593	491	18296	7273	1315	449	**Overall accuracy:**	
Producer Accuracies	98.13%	17.11%	85.82%	75.92%	68.21%	72.83%		**83.41%**

Appendix B

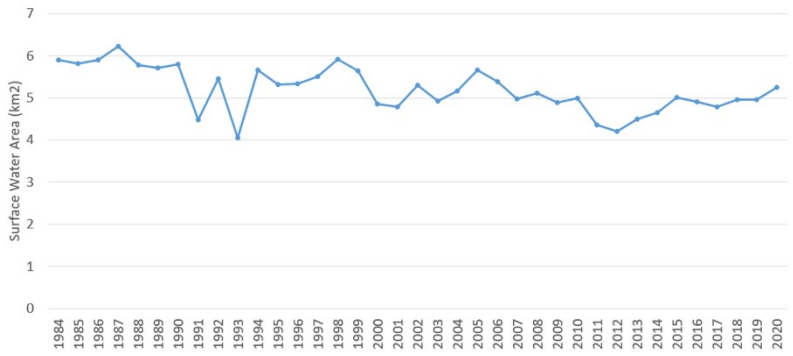

Figure B1:
Sum of surface water area of major channels in the outer Slave River Delta, 1984-2020

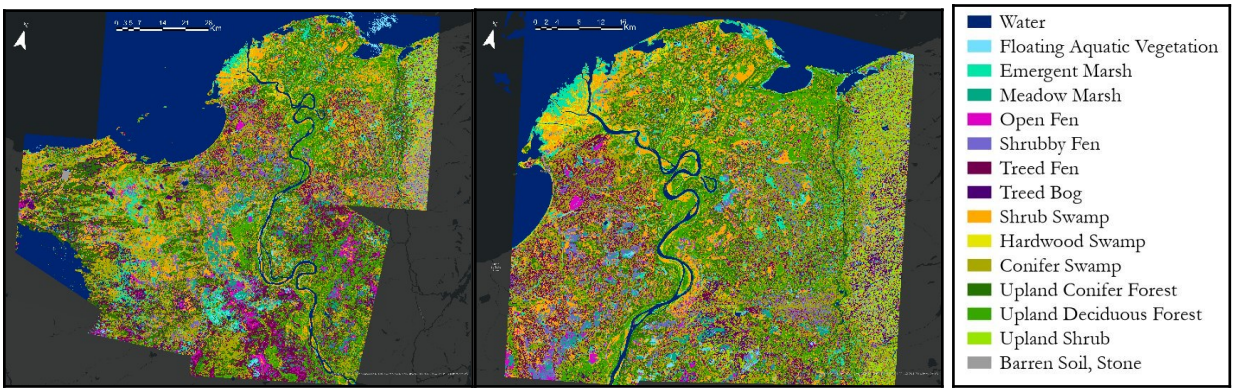

Figure B2.
ABoVE enhanced wetland classification images for 2007 (left) and 2017 (right).

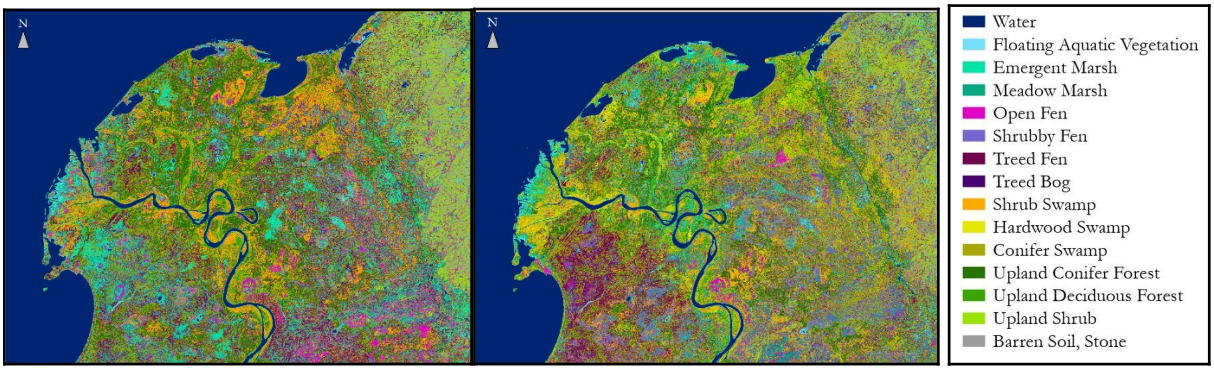

Figure B3.
Enhanced wetland classification training results for 2008 (left) and 2017 (right) in the SRD.

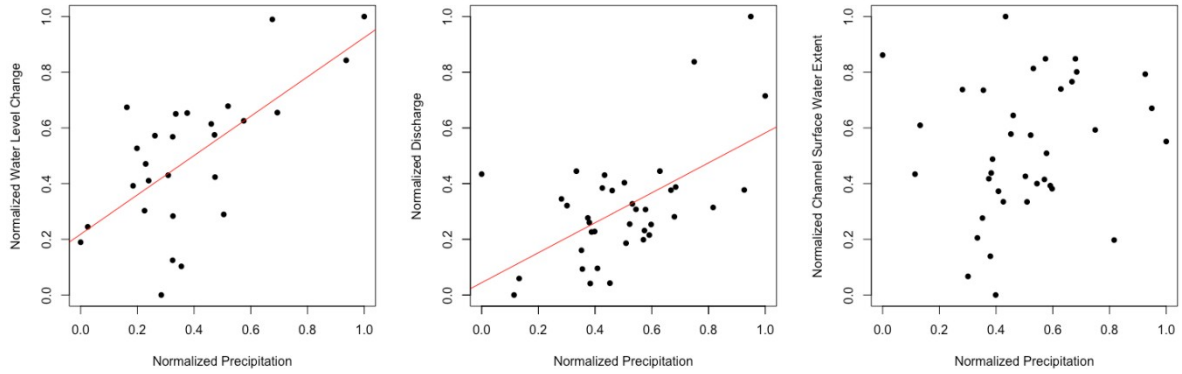

Figure B4.

Least-squares linear regression scatter plots showing normalized annual values for Slave River watershed precipitation as a predictor of normalized annual Slave River discharge (left, slope = 0.706), Great Slave Lake water level changes (middle, slope = 0.538), and total surface water area of outer SRD water channels with insignificant slope to be 0.192 (right).

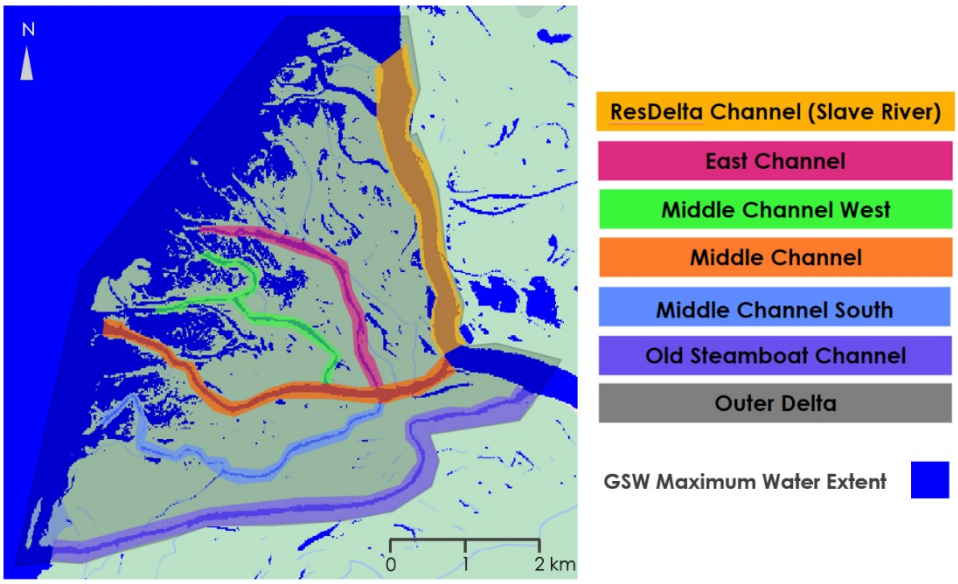

Figure B5.

Polygons representing the individual SRD channels and the outer delta, overlaid on the GSW maximum water extent layer. Basemap: Google.